Nanoscale

ROYAL SOCIETY OF CHEMISTRY

PAPER

View Article Online
View Journal | View Issue

Cite this: *Nanoscale*, 2022, **14**, 9781

Calibration and standardization of extracellular vesicle measurements by flow cytometry for translational prostate cancer research†

Yohan Kim,[a] Edwin van der Pol,[b,c,d] Ali Arafa,[a] Ishwor Thapa,[e] Cameron J. Britton,[a] Jorgena Kosti,[a] Siyang Song,[a] Vidhu B. Joshi,[f] Ree M. Erickson,[a] Hesham Ali[e] and Fabrice Lucien *[a]

Extracellular vesicles (EVs) are microscopic particles released naturally in biofluids by all cell types. Since EVs inherits genomic and proteomic patterns from the cell of origin, they are emerging as promising liquid biomarkers for human diseases. Flow cytometry is a popular method that is able to detect, characterize and determine the concentration of EVs with minimal sample preparation. However, the limited awareness of the scientific community to utilize standardization and calibration methods of flow cytometers is an important roadblock for data reproducibility and inter-laboratory comparison. A significant collaborative effort by the Extracellular Vesicle Flow Cytometry Working Group has led to the development of guidelines and best practices for using flow cytometry and reporting data in a way to improve rigor and reproducibility in EV research. At first look, standardization and calibration of flow cytometry for EV detection may seem burdensome and technically challenging for non-academic laboratories with limited technical training and knowledge in EV flow cytometry. In this study, we build on prior research efforts and provide a systematic approach to evaluate the performance of a high sensitivity flow cytometer (herein Apogee A60-Micro Plus) and fine-tune settings to improve detection sensitivity for EVs. We performed calibration of our flow cytometer to generate data with comparable units (nanometers, MESF). Finally, we applied our optimized protocol to measure the concentrations of prostate-derived EVs in healthy individuals and prostate cancer patients. In conclusion, our proof-of-feasibility study can serve as a scientific and technical framework for other groups motivated in using flow cytometry for EV research.

Received 28th February 2022,
Accepted 25th May 2022

DOI: 10.1039/d2nr01160c

rsc.li/nanoscale

Introduction

Extracellular vesicles (EVs) are emerging as promising liquid biomarkers for the management of human cancers.[1] The International Society for Extracellular Vesicles (ISEV) endorses EVs as a generic term for particles naturally released from the cell that are delimited by a lipid bilayer and cannot replicate, *i.e.* do not contain a functional nucleus.[2] EVs have a wide size range between 30 nanometers and 5 micrometers and they are abundantly released in biofluids such as blood and urine.[3] Having the capacity to detect EVs specifically released from tumor cells offers numerous benefits for cancer diagnosis, early-detection of disease recurrence and monitoring response to therapy. In line with this, the development of EV-based tests for prostate cancer has been an active area of investigation because of high incidence rates and limited performance of current diagnostic tools.[4–6] Prostate-specific antigen (PSA) screening has improved early-diagnosis of prostate cancer, but the poor specificity of PSA test leads to overdiagnosis and unnecessary invasive tissue biopsy. Therefore, there is a strong need to develop non-invasive tools to identify men with clinically significant prostate cancer and avoid unnecessary biopsies for men with no cancer or indolent cancer.[4,5]

While the multifaceted role and regulation of EVs is heavily studied, great progress has been made in the development and optimization of methods to detect, characterize, and isolate EVs.[7] Flow cytometry (FCM) is a commonly used technique for

[a]*Department of Urology, Mayo Clinic, Guggenheim 4-97, 200 1st Street SW, Rochester, MN, 55901, USA. E-mail: Lucien-matteoni.fabrice@mayo.edu*
[b]*Department of Biomedical Engineering and Physics, Amsterdam University Medical Center, Amsterdam, The Netherlands*
[c]*Laboratory Experimental Clinical Chemistry, Amsterdam University, Medical Center, Amsterdam, The Netherlands*
[d]*Vesicle Observation Center, Amsterdam University Medical Center, Amsterdam, The Netherlands*
[e]*College of Information Science and Technology, University of Nebraska at Omaha, USA*
[f]*Department of Biochemistry and Molecular Biology, Mayo Clinic, Rochester, MN, USA*

† Electronic supplementary information (ESI) available. See DOI: https://doi.org/10.1039/d2nr01160c

single EV analysis. FCM holds several advantages over other common methods such as electron microscopy and nanoparticle tracking analysis. FCM allows for high-speed detection of millions of particles (≥100 nm) within a few minutes from a small volume and without the need for EV enrichment or isolation. Furthermore, FCM combines light-scatter detection of particles with fluorescence immunophenotyping that gives the opportunity to estimate EV diameters as well as concentrations of EVs released by a cell population of interest. These unique capabilities have driven the use of FCM to assess the clinical utility of EVs as cancer biomarkers.[8–12]

Nevertheless, several challenges remain to be addressed before unleashing the full capabilities of EV detection with FCM. The small size of EVs, low abundance of surface antigens and biophysical similarities with EV-like particles are important hurdles in EV detection. Conventional and high-sensitivity flow cytometers vary in their performance to resolve EVs above the background noise using light-scatter or fluorescence detection.[13–16] Accordingly, several groups have been investing in optimizing FCM hardware and pre-analytical and analytical conditions to reliably detect EVs.[14,17–21] Furthermore, an international collaborative effort led by the EV-FCM Working Group has raised awareness towards the calibration and standardization of flow cytometric detection of EVs to maximize rigor and reproducibility in data acquisition, analysis, and reporting.[15,22–24]

In this study, we described a systematic approach for standardization of acquisition parameters for side-scatter detection of EVs and other particles from cell-depleted plasma and urine. We demonstrated that, without in-depth technical training and knowledge in EV flow cytometry, standardization and calibration of EV flow cytometry is feasible by building on prior research efforts. To fulfill the prerequisites of rigor and transparency established by the EV-FCM Working Group, we performed calibration of our flow cytometer and transformed side-scatter and fluorescence intensities in standardized units (particle diameter and MESF values). Next, we determined optimal pre-acquisition and data acquisition settings such as sample dilution, illumination wavelength power, triggering threshold, and flow rates. Finally, we applied our optimized protocol for flow cytometric quantification and characterization of EVs in plasma and urine of healthy individuals and prostate cancer patients. Our optimized workflow will help us evaluate the clinical value of circulating extracellular vesicles for prostate cancer diagnosis in a reliable manner. Furthermore, in synergy with the EV flow cytometry community efforts, our work will facilitate the conduct of multicenter translational studies using flow cytometry.

Materials and methods

Blood and urine collection

Blood and urine samples were collected from localized prostate cancer patients and benign individuals. Demographics and clinicopathological characteristics can be found in Table 1. All samples were collected with approved Mayo Clinic IRB (19-006675, 21-004451). All urine samples were processed within 30 minutes post-collection. Blood samples were processed within 1 hour post-collection. Whole patient blood (40 mL) was drawn using a 21 G needle in EDTA-coated vacutainers (BD Biosciences, San Jose, CA). Vacutainers were centrifuged at 2500*g* (κ factor – 9153), 20 °C with low break for 15 minutes with Sorvall Legend 1XR centrifuge (Thermo Fisher Scientific, Waltham, MA) and top layer of plasma was transferred into 15 mL conical centrifugal tubes without disturbing the buffy coat (1 mL was left above the buffy coat). Plasma was centrifuged again at 2500*g* (κ factor – 9153), 20 °C for 15 minutes to obtain platelet-free plasma (PFP). Removal of platelets was confirmed by nanoscale flow cytometry by staining for CD61 using CD61-APC antibodies (HIP8 clone).[17] Top layer of plasma (approximately 1 mL left from bottom) was transferred to cryovials and stored at −80 °C without snap freezing and until further use. First-catch urine was collected using Collipee collection device (Novosanis, Belgium). 20 mL of urine was transferred to a 50 mL conical tube and centrifuged at 3000*g* (κ factor – 9153), 20 °C with low break for 15 minutes. 15 mL of supernatant was transferred to cryovials (1 mL per vial) and stored at −80 °C until further analysis. A separate cohort of 20 widely metastatic CRPC (mCRPC) (*i.e.* patients with >3 metastatic lesions) detected by conventional CT and/or bone scan and with a PSA level above 2.0 ng ml^{-1} was used to compare EV levels between localized PCa and metastatic PCa patients (IRB #21-004451).

Table 1 Demographics and clinicopathological characteristics of patients

	Patient cohort		
	BPH	Localized PCa	Metastatic PCa
Number of patients	35	85	20
Age			
Median (min to max)	63 (43–76)	66 (50–86)	66 (55–76)
Prostate specific antigen levels (ng mL^{-1})			
Median (min to max)	6.7 (1.0–17.6)	6 (1.4–29)	8.9 (0.88–117)
Gleason scores			
Gleason score 0	35	NA	NA
Gleason score 3 + 3	NA	22	NA
Gleason score 3 + 4	NA	38	NA
Gleason score 4 + 3	NA	16	NA
Gleason score 4 + 4	NA	3	NA
Gleason score > 8	NA	6	NA
Number of lesions			
Median (min to max)	NA	NA	Unknown

Side scatter calibration of flow cytometry

Side scatter was calibrated with Rosetta Calibration beads (#Cal002, Exometry, The Netherlands) and Rosetta Calibration software (version v1.24 purchased license from Exometry, The Netherlands) according to manufacturer's instructions (Exometry, The Netherlands). Briefly, a mixture of polystyrene beads of known size and refractive index was analyzed and side scatter intensities in arbitrary units were converted in

nanometers using Mie theory modeling.[16,25] To estimate the size of an extracellular vesicle, we assumed that polystyrene beads have a refractive index of 1.633 and double distilled water as sheath fluid has a refractive index of 1.343 at an illumination wavelength of 405 nm. For EVs, we assumed a core refractive index of 1.38, a shell refractive index of 1.48 and a shell thickness of 4 nm.[12] For label-free identification of EVs from lipoproteins, we determined the diameter and refractive index of each particle detected by flow cytometry using the Flow-Scatter Ratio (Flow-SR) as described previously.[25] Briefly .fcs files were imported into Rosetta Calibration software to convert side scatter intensities into diameter. Then, files were transferred to the Flow-SR software to measure levels of particles below and above refractive index of 1.45.[25,26]

Flow cytometry acquisition settings

Each sample was analyzed on Apogee A60-Micro Plus (A60MP, Apogee Flow Systems Inc., Northwood, UK) equipped with 3 excitation lasers (405, 488, 638 nm) and 9 detectors. Default configuration for the A60MP included: a 405 nm excitation laser set at 70 mW for side scatter detection, a side scatter triggering threshold of 2300 arbitrary units (corresponding to a side scattering cross section of 19 nm^2 and an EV diameter of 188 nm with a core refractive index of 1.38 and a shell refractive index of 1.48), a flow rate of 0.75 μl min^{-1} and an acquisition time of 60 seconds. Before each run, a blank sample with DPBS was run to ensure a count rate < 100 events per second. Each sample was run in three technical replicates for 60 seconds. The laser power, triggering threshold and flow rate were adjusted as described in the manuscript. Each week, the A60MP underwent a quality control procedure including a run with a mix of fluorescent polystyrene and silica polydisperse beads (Apogee bead mix #1493, Apogee Flow Systems) to control for instrument sensitivity and flow rate stability. Data analysis was performed in FlowJo version 10.6.1. Number of detected events, sample dilution, flow rate and acquisition time were used to determine particle concentration. For a detailed description of the flow cytometer specifications, pre-analytical and analytical procedures, please refer to the MIFlowCyt-EV report (ESI†).

Fluorescence intensity calibration

MESF reference values for each population of Alexa fluor 488 (AF488) and 647 (AF647) beads, along with acquired channel statistics for each population were log-transformed before performing linear regression (Quantum™ Alexa Fluor488 MESF and Alexa Fluor647 MESF, Bangs Laboratories Inc., Fishers, Indiana). Log transformed raw data was then converted to MESF units using the obtained slope and intercept (Fig. S1†).

Antibody conjugation and preparation

PSMA (3/E7, Creative Biolabs) and STEAP1 (SMC1, Mayo Clinic Hybridoma Core) antibodies were labeled with Alexa Fluor 647 (AF647) and 488 (AF488) antibody labeling kits (Thermo Fisher Scientific, Waltham, MA) respectively. Degree of antibody labeling (DOL) was measured using a Nanodrop One C spectrophotometer (Fisher Scientific). Degree of labeling (DOL) for PSMA and STEAP1 was 3.2 and 3.6 respectively. The antibodies were then stored at 4 °C for future use. For sample preparation, antibodies were centrifuged at 17 000*g* for 30 minutes at 20 °C to remove any fluorescent antibody aggregates. Antibodies were diluted to DPBS to prepare working antibody solution with the desired concentrations and kept in ice.

Immunophenotyping of EVs

Both plasma and urine samples were thawed at 37 °C for 2 minutes. Samples (1 ml) were centrifuged at 13 000*g* for 5 minutes at room temperature to remove any aggregates and 900 μL of supernatant was transferred into a new Eppendorf tube. All plasma samples were pre-diluted in sterile DPBS (Thermo Fisher Scientific, Waltham, MA) as indicated in the manuscript. Urine samples were not pre-diluted prior to analysis. 10 μL of PSMA-AF647 and STEAP1-AF488 antibodies with desired concentrations (6 μg mL^{-1} final concentration for both antibodies) were plated to a well of 96-well V-plate, then 10 μL of pre-diluted plasma or urine samples were added to the antibody mixture, which makes a total volume of 30 μL. The antibody-biofluid mixture was incubated in dark for 30 minutes at room temperature to label prostate specific EVs with antibodies. Each well was filled with 170 μL of DPBS to end the incubation and proceed to sample analysis. Unstained PFP was used to gate and count fluorescent events for each antibody. To determine the specificity of antibody staining, cell- and plasma-derived EVs were incubated with 0.1% SDS in the dark and at room temperature for 30 minutes. 180 μL of DPBS was added to stop incubation and then the sample was analyzed with A60MP.

Cell lines and transfection

Human HEK293T (ATCC, Manassas, VA, USA) were maintained in a humidified incubator at 5% CO_2. HEK293T cells were cultured in high glucose DMEM (Corning, New York, NY, USA) with 10% fetal bovine serum (Thermo Fisher Scientific, Waltham, MA) and 5% penicillin and streptomycin (Thermo Fisher Scientific, Waltham, MA). Cells were cultured at 70–80% confluency in a 6-well plate (Thermo Fisher Scientific, Waltham, MA) and transiently transfected with CD63-pEGFP C2 (#62964) gag-GFP (#80605) and pEGFP-C1 (#54759) constructs purchased from Addgene. To collect cell-derived EVs, cells were cultured in serum-free media for 48 hours. Conditioned medium was collected and centrifuged twice at 2500*g* (κ factor – 9153), 20 °C for 15 minutes with max break. 1 mL of EV-containing supernatants was aliquoted in cryovials and stored at −80 °C until further use.

Ultracentrifugation-based EV depletion from human plasma

Patient plasma samples (4 mL per sample) in Ultra-Clear centrifuge tubes (Beckman Coulter, Inc., Brea, CA) were centrifuged at 20 000*g* (κ factor – 48) for 40 minutes (20 °C) and 100 000*g* (κ factor – 48) for 16 hours (4 °C) in a Beckman Coulter (Brea, CA) Optima XPN-100 ultracentrifuge using a SW

55 Ti rotor to deplete EVs. After the process of sequential centrifugation, plasma samples were diluted in DPBS. 10 μL of diluted plasma samples were incubated with anti-PSMA and STEAP1 antibodies in dark at room temperature for 30 minutes followed by adding 180 μL of DPBS to the mixture. The prepared sample was run with A60MP.

Statistical analysis

Student *t*-test (parametric), Mann–Whitney test (non-parametric) was employed to compare two groups. One-way ANOVA (parametric) and Kruskal–Wallis (non-parametric) tests were used to compare three or more groups. Linear regression analysis was conducted to determine correlation between continuous variables (EV concentrations). The interquartile range method was used to exclude outliers in correlation tests. The results were considered significant for p values < 0.05. p values were either specified in the figure or denoted as asterisk: $*p < 0.05$, $**p < 0.01$, $***p < 0.001$, $****p < 0.0001$. All data were analyzed and plotted in GraphPad Prism 9.0.1.

Results

Determination of the linear relationship between particle concentration and dilution

Swarm detection is an important factor in single particle discrimination by flow cytometry that can lead to false enumeration of submicron particles within particle-rich biofluids, such as plasma and serum.[27] At high concentration, multiple particles below the detection limit can run continuously through the laser beam and be counted as single particle. As recommended by the EV Flow Cytometry Working Group, serial dilutions of samples must be performed to determine whether the measured particle concentration scales linearly with sample dilution.[22] Platelet-free plasma and cell-free urine of three prostate cancer patients were serially diluted in PBS and particle concentration was measured using side-scatter detection on the A60MP flow cytometer (Fig. 1).

To determine the linear range for particle concentrations measured by the A60MP, we calculated *R*-squared values for successive sets of data points, and observe the range for which perfect linearity was maintained across all dilutions. For PFP, linear quantification of particles was lost when concentration exceeded 4.8×10^8 particles per ml for PFP_1, 5.8×10^8 particles per ml for PFP_2 and 5.0×10^8 particles per ml for PFP_3 (Fig. 1A–C). This represented a 40-fold dilution for PFP_1 and PFP_3 and a 160-fold dilution for PFP_2. Mean particle concentration at the upper limit was 5.8×10^8 particles per ml, which corresponds to a mean event rate of 6.5×10^3 events per s. At a particle concentration below $\sim 1.0 \times 10^7$ particles per ml (event rate ~ 125 events per s), the measured concentration exceeded the concentration expected from the dilution due to the presence of background noise (particle and optical noise), as verified with the buffer-only control (~89 ± 35 particles per s) (Fig. S3†). Swarm detection can also be confirmed by measuring side scatter intensities of particles where median scattering intensity increased with decreasing dilutions.[27] Loss of linearity in side scatter intensities was observed at low dilution for PFP_1 and _2 which is in line with loss of linearity observed for particle concentration (Fig. 1A–C). Therefore, particle concentrations of clinical samples under 5.8×10^8 particles per ml (6.5×10^3 events per s) are optimal to achieve linearity.

Patient-matched urine samples were run with similar settings as plasma samples (Fig. 1D–F). At the lowest dilution (4-fold), the particle concentration did not exceed 1.6×10^8 particles per ml corresponding to an event rate of 2.0×10^3 events per s (Urine_3). Hence, the concentration of particles in urine was significantly lower than in plasma. Upon serial dilution, perfect ($R^2 = 0.999$, $p < 0.0001$) linearity was achieved except for Urine_1 where linearity was lost at a particle concentration below 1.6×10^7 particles per ml (event rate 199 events per s). No difference was observed in median side scatter intensities across all dilutions which confirmed the absence of swarm effect in particle analysis from urine.

PFP from 20 prostate cancer patients were analyzed at a 200-fold dilution (Fig. 1G). Median particle concentration measured by the A60MP was 2.2×10^8 particles per mL (min = 2.3×10^7; max = 1.2×10^9). By using the upper detection limit for concentration of 5.8×10^8 particles per mL, 20% samples exceeded the upper detection limit for concentration. Using a 20-fold dilution of urine from 20 prostate cancer patients, median particle concentration was 3.1×10^7 particles per mL (min = 1.1×10^7; max = 1.1×10^8) with no sample exceeding the upper detection limit for particle concentration (Fig. 1H).

Altogether, these data indicate that submicron particles can be rigorously quantified from cell-depleted plasma and urine. For our A60MP flow cytometer, we obtained a linear relation between particle concentration and sample dilution below a concentration of 5.8×10^8 particles per mL, suggesting that minimal dilution factor for urine sample is acceptable to keep particle concentrations in the detection range of the flow cytometer. For plasma, a 200-fold dilution is an acceptable starting dilution but some samples exceeding the upper detection limit might need higher dilution.

Detection of fluorescent recombinant EVs spiked-in biofluids

To assess the sensitivity of the A60MP for detecting EVs, we, per Fig. S2A,† generated recombinant EVs (rEVs) *in vitro* from HEK293T transfected with an expression vector coding for the fluorescent reporter GFP, the EV-enriched cell-surface marker CD63 tagged with GFP or the viral protein Gag tagged with GFP. EVs released by cells transfected with Gag-GFP construct are enriched in GFP bound to the inner leaflet of the plasma membrane, which can be used as reference biological material for EV flow cytometry experiments.[28] Analysis of culture medium-derived rEVs by flow cytometry in Fig. S2B† showed higher percentage of EVs positive for Gag-GFP (~79%) compared to CD63-GFP (41%) and GFP (18%). Fig. S2C† shows that Gag-GFP-positive EVs have higher mean fluorescence

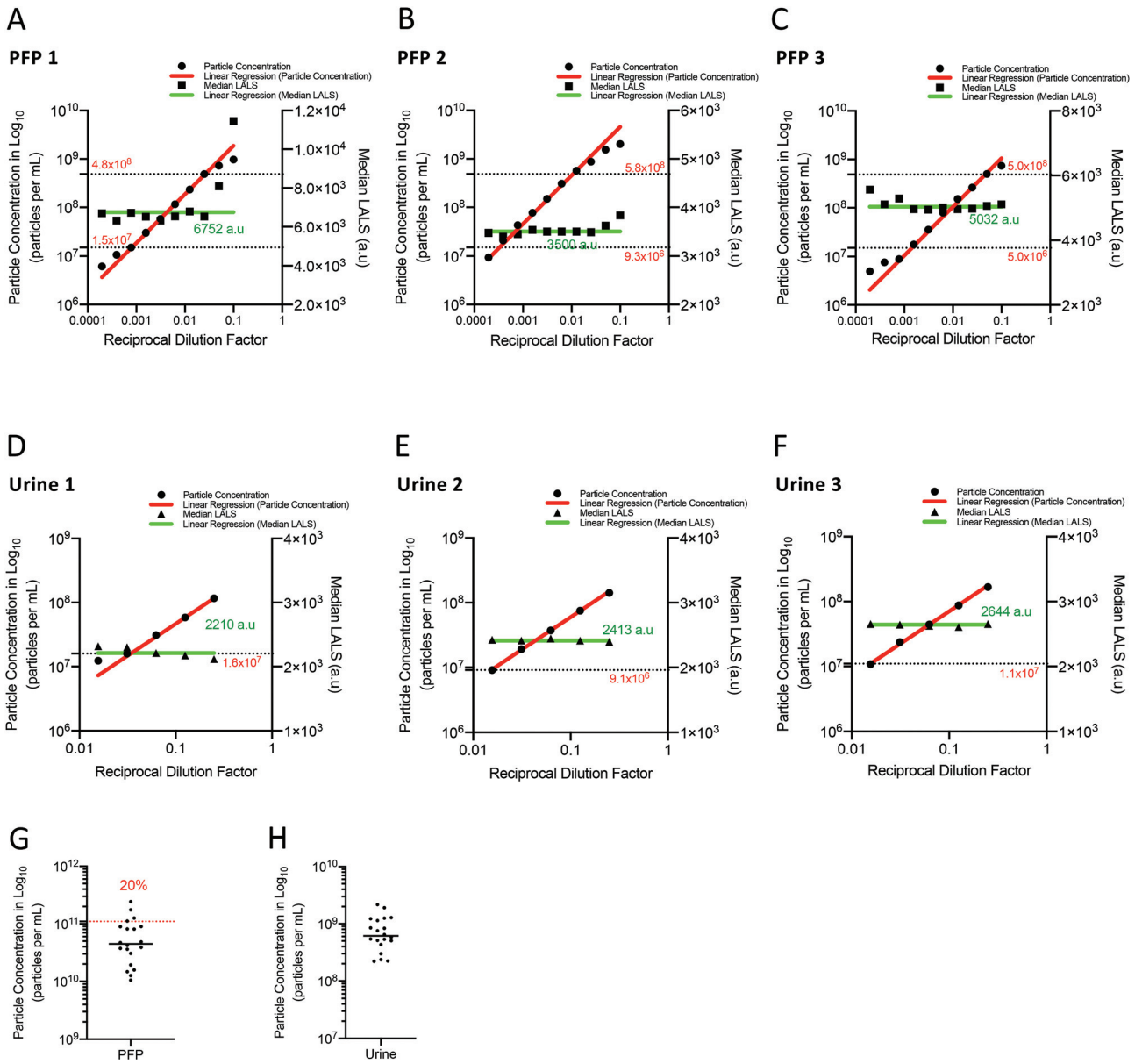

Fig. 1 Determination of the linear detection range of particles from platelet-free plasma and cell-free urine by nanoscale flow cytometer. (A–C) Concentrations of particles and median side scatter measured in serial dilution of additional platelet-free plasma samples (N = 3). Particle concentrations, median side scatters and dilution factors are presented in logarithmic scale. Perfect linear regression curve (R^2 = 1) for particle concentrations and median side scatters are presented in red (r = 1) and green (r = 1). (D–F) Concentrations of particles and median side scatter measured in serial dilution of additional cell-free urine samples (N = 3). Particle concentrations, median side scatters and dilution factors are presented in logarithmic scale. Perfect linear regression curve (R^2 = 1) for particle concentrations and median side scatters are presented in red (r = 1) and green (r = 1). (G) Concentrations of particles measured in a 200-fold dilution of platelet-free plasma samples (N = 20). Dotted line in red indicates the maximum particle concentration for linear detection. (H) Concentrations of particles measured in a 20-fold dilution of urine (N = 20).

intensity compared to GFP-EVs and CD63GFP-EVs. We also employed refractive index-based discrimination (Flow-Scatter Ratio or Flow-SR) to compare particle refractive index (RI) of EVs ≥ 200 nm released from HEK293T Gag-GFP-positive or wild-type cells (Fig. S2D†).[25] As expected, most EVs (92%) release from wild-type cells fell under RI < 1.45. Similarly, 95% of GagGFP-positive EVs showed a RI < 1.45 which confirms that Gag-GFP-positive EVs share similar biophysical properties to wild-type EVs. Serial dilutions of rEVs (Gag-GFP-EVs) were spiked-in PFP and urine and concentrations were recorded to determine the lower concentration for linear quantification of rEVs (Fig. S2E–H†). Linear quantification of rEVs was achieved down to 4.6×10^4 EVs per mL for PFP (r = 0.998, p < 0.0001, 0.062% of total particles) and 3.0×10^4 EVs per mL for urine (r = 0.997, p < 0.0001, 0.51% of total particles).

Impact of acquisition parameters on side scatter detection of particles and rEVs from platelet-free plasma and cell-free urine

Power of illumination laser positively correlated with side scatter detection of particles and rEVs in platelet-free plasma and cell-free urine. By using rEVs spiked-in plasma and urine from three prostate cancer patients, we compared four different powers (70, 100, 150 and 200 mW) of the 405 nm excitation laser for side scatter detection and quantification of particles and rEVs. Fig. 2A shows total particle concentrations measured in PFP samples positively correlated with laser power (PFP_1 $r = 0.993$ and $p < 0.01$, PFP_2 $r = 0.993$ and $p < 0.01$, PFP_3 $r = 0.944$ and $p < 0.05$). In contrast to total particles, concentrations of rEVs modestly increased at 100 mW compared to 70 mW and reached a plateau at 150 mW (Fig. 2B). In Fig. S3,† particle measurement from filtered PBS also showed higher number of particles detected with increasing laser power but remained much lower (<24-fold) than PFP particle concentration. A laser power of 100 mW impacted very slightly (~10%) on the measurement of particle and rEV concentrations while higher laser powers led to significant increase in both particle and rEV concentrations measured (Fig. 2C). Concentrations of particles detected were increased by 102% and 129% at a laser power of 150 mW and 200 mW while levels of rEVs were only increased by 39% and 35% respectively compared to a laser power of 70 mW. The loss of linearity in rEV concentrations measured at high laser power can result from photobleaching of GFP fluorophores 29345328. We calculated mean fluorescence intensity of rEVs and found a reduction by ~15% at laser power above 150 mW (Fig. S3D†). This suggests that photobleaching of dimly fluorescent GagGFP-positive EVs can shift their fluorescence intensity below the minimum detectable signal-to-noise ratio of the instrument resulting in loss of linearity in the relationship between laser power of GagGFP-positive EV concentrations measured (Fig. 2B). Similar to PFP, increase of laser power was associated with higher particle and rEV concentrations measured in urine (Fig. 2D). While detectable levels of rEVs increased by 39% in PFP at 150 mW, it increased by 58% in urine compared to the levels of rEVs measured at 70 mW.

To validate our findings, we measured side scatter intensities of NIST traceable 80 nm polystyrene beads (Fig. S4A†). We observed a positive correlation between laser power and side scatter intensities ($r = 0.999$, $p < 0.01$) (Fig. S4B†). Positive correlation was also found with laser power and particle concentration ($r = 0.990$, $p < 0.01$). At 200 mW, a concentration of 5.9×10^7 beads per milliliter was detected which is close to the known concentration of 6.5×10^7 beads per milliliter (±10%). These data demonstrate that increasing laser power for side scatter particle detection improves sensitivity for smaller particles resulting in higher particle concentration measured. Furthermore, recombinant EVs spiked-in biofluids are a suitable biological tool to determine instrument sensitivity, risk of photobleaching and optimize data acquisition settings for EV quantification from blood and urine.

Determination of optimal triggering threshold for side scatter detection of particles and rEVs. The triggering threshold is another critical aspect of single particle analysis, because it determines on the one hand the number of included background events and on the other hand the signal level of the dimmest detectable particle. To determine the optimal side scatter triggering strategy, we compared three different triggering thresholds 1800, 2000, and 2300 arbitrary units. Number of events acquired with PBS was significantly increased with reduced triggering threshold reaching ~2699 events per second at a threshold of 1800 a.u. (Fig. S5A–C†). High event rate with PBS likely results from acquisition of electronic and optical noise. Similarly, total particle concentration from PFP was significantly increased by 64% at a threshold of 1800 a.u. compared to 2300 a.u. (Fig. 3A–C). In contrast, levels of rEVs only increased by 29% at a threshold of 1800 a.u. In urine, total particle concentration increased by 105% at a threshold of 1800 a.u. compared to 2300 a.u. while rEV concentrations measured only increased by 21% (Fig. 3D).

Impact of flow rate on side scatter detection of particles and rEVs. The flow rate with the optimal dilution together controls

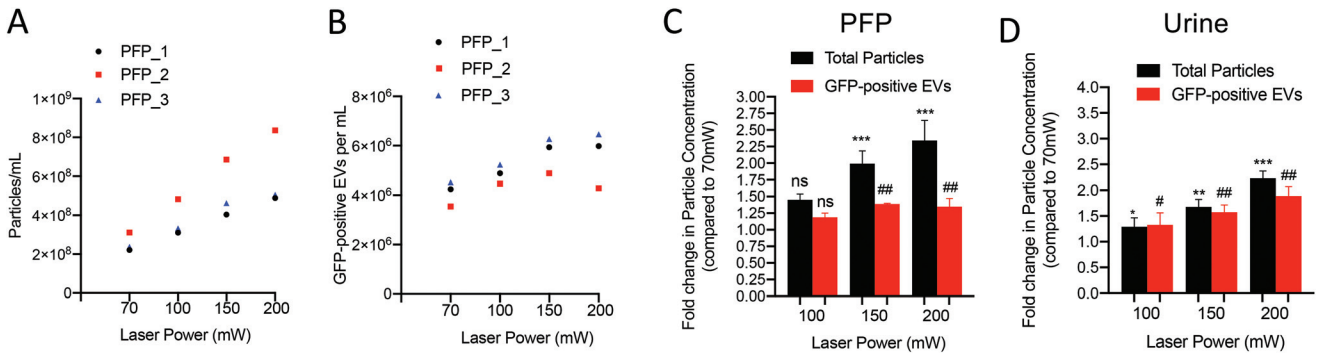

Fig. 2 Impact of laser power on side scatter detection of particles and EVs from platelet-free plasma and cell-free urine. (A and B) Concentrations of total particles and GFP-positive rEVs in rEV spiked-in PFP samples ($N = 3$) measured in different laser powers. Laser powers are presented in milliwatts (mW). Dotted line indicates the maximum particle concentration for linear detection of particles. (C and D) Fold changes in detection levels of total particles and rEVs from rEV spiked-in PFP ($N = 3$) and urine ($N = 3$) samples measured in different laser powers. Laser powers are presented in milliwatts (mW).

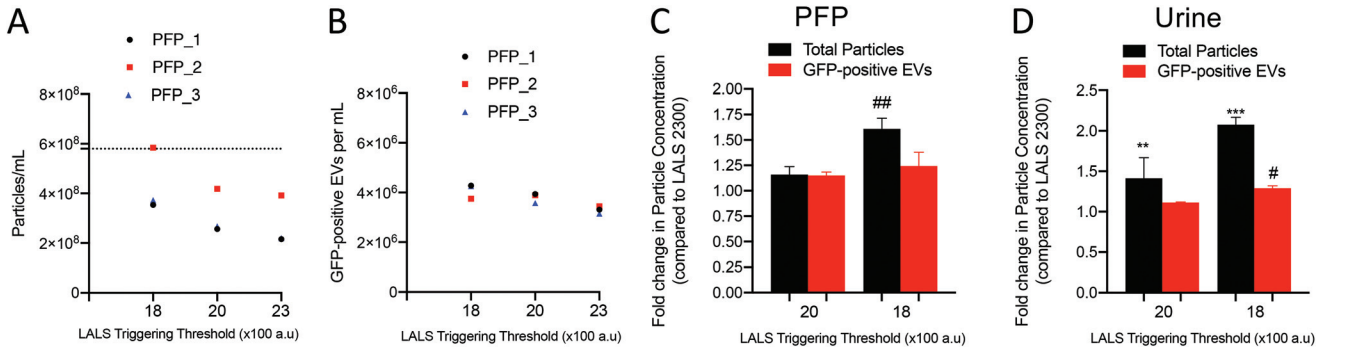

Fig. 3 Impact of acquisition parameters on side scatter detection of particles and EVs from platelet-free plasma and cell-free urine. (A and B) Concentrations of total particles and GFP-positive rEVs in rEV spiked-in PFP (N = 3) samples measured in different triggering thresholds. Triggering threshold is presented in arbitrary unit (a.u.). Dotted line indicates the maximum particle concentration for linear detection of particles. (C and D) Fold changes in detection levels of total particles and rEVs from rEV spiked-in PFP (N = 3) and urine (N = 3) samples measured in different triggering thresholds. Particle concentrations measured in triggering thresholds 1.8×10^3 and 2.0×10^3 a.u. were normalized to the one measured in triggering thresholds 2.3×10^3 a.u.

the sample volume passing through the laser beam. A low flow rate is usually associated with higher sensitivity for single particle analysis because less particles are running simultaneously through the interrogation point thereby limiting the incidence of swarm detection.[17] Therefore, different flow rates (0.75, 1.50 and 3.00 μl min^{-1}) were evaluated in terms of particle concentration measured and variance between technical and biological replicates. For PBS alone, the event rate was proportional to the flow rate and measured particle concentration was unaffected (Fig. S5D–F†). For PFP, a flow rate of 0.75 or 1.50 μl min^{-1} led to similar particle and rEV concentrations measured by A60MP (Fig. 4A–C). In contrast, a flow rate of 3.0 μl min^{-1} was associated with a significant decrease in both particle and rEV concentrations (Fig. 4B and C). A decrease of 30% in rEV concentrations was observed in PFP samples analyzed at 3.0 μl min^{-1} compared to 0.75 μl min^{-1} (Fig. 4D). A flow rate of 1.5 μl min^{-1} was associated with better stability between replicates with a coefficient of variation of 4.2% ± 1.8% (Fig. 4E). A flow rate of 0.75 and 3.0 μl min^{-1} showed a coefficient of variation of 9.3% ± 9.9% and 17.4% ± 15.7%. Particle and EV quantification from urine was not affected by flow rate (Fig. 4F). However, a flow rate of 1.5 and 3.0 μl min^{-1} resulted in smaller variance between replicates with a coefficient of variation of 7.43% ± 6.47% and 6.0% ± 1.59%, respectively (Fig. 4G).

Altogether, our data showed that acquisition parameters and particle abundance can significantly influence sensitivity and enumeration of particles measured from platelet-free plasma. Standardization of acquisition parameters and selection of optimal settings are required to have best sensitivity for EV quantification while maintaining the linearity in particle detection by the flow cytometer. Given the major differences in particle concentration in blood and urine, different acquisition parameters may be used to provide the best detection sensitivity for single particle analysis. In our environment, optimal settings for PFP analysis included a 405 nm laser set at 70 mW, a flow rate of 0.75 μl min^{-1} and a triggering threshold on side-scatter of 2300 a.u. Analysis of urine-derived EVs was optimal with a 405 nm laser set at 150 mW, a flow rate of 3.0 μl min^{-1} and a triggering threshold at 2300 a.u.

Calibration of side scatter detection of particles by nanoscale flow cytometry

After having defined the optimal acquisition parameters for particle detection in blood and urine using flow cytometry, we calibrated our flow cytometer and report scatter and fluorescence intensities in standardized measurement units. This is in accordance with the large collaborative effort to improve rigor and reproducibility in single particle detection by flow cytometry.[29] Acquisition settings for PFP included a 405 nm excitation laser set at 70 mW and a side scatter triggering threshold set at 2300 arbitrary units. A mixture of fluorescent and non-fluorescent polystyrene beads (Rosetta Calibration) was analyzed, and side scatter intensities were recorded and converted in standardized units using Mie Theory-based scatter modeling.[16] The A60MP successfully detected polydisperse polystyrene beads ranging from 120 nm to 400 nm while larger polystyrene beads in the mixture saturated the detector (Fig. S6A†). The side scattering intensity to diameter relationship showed that 200 nm polystyrene beads (Refractive index = 1.63) scatter as much light as an EVs of 730 nm (Refractive index core = 1.38; Refractive index shell = 1.48; shell thickness = 4 nanometers). Polystyrene beads of 80 nm diameter (RI = 1.63) have similar side scatter intensities as an EV of 158 nm ± 10 nm (RI core = 1.38; RI shell = 1.48; shell thickness = 4 nm) (Fig. S6B†). Side scatter intensities generated by rEVs mainly fell in the range of 100–125 nm polystyrene beads with a peak at 2822 arbitrary units corresponding to a diameter of 199 nm (Fig. S6C†). In our A60MP system, a side scatter triggering threshold of 2300 a.u. corresponds to a scattering cross section of 19 nm^2 and an EV diameter of 188 nm, given the assumed refractive index distribution of an EV is correct. For urine, acquisition settings included a 405 nm excitation laser set at 150 mW. A side scatter triggering threshold set at 2300 arbi-

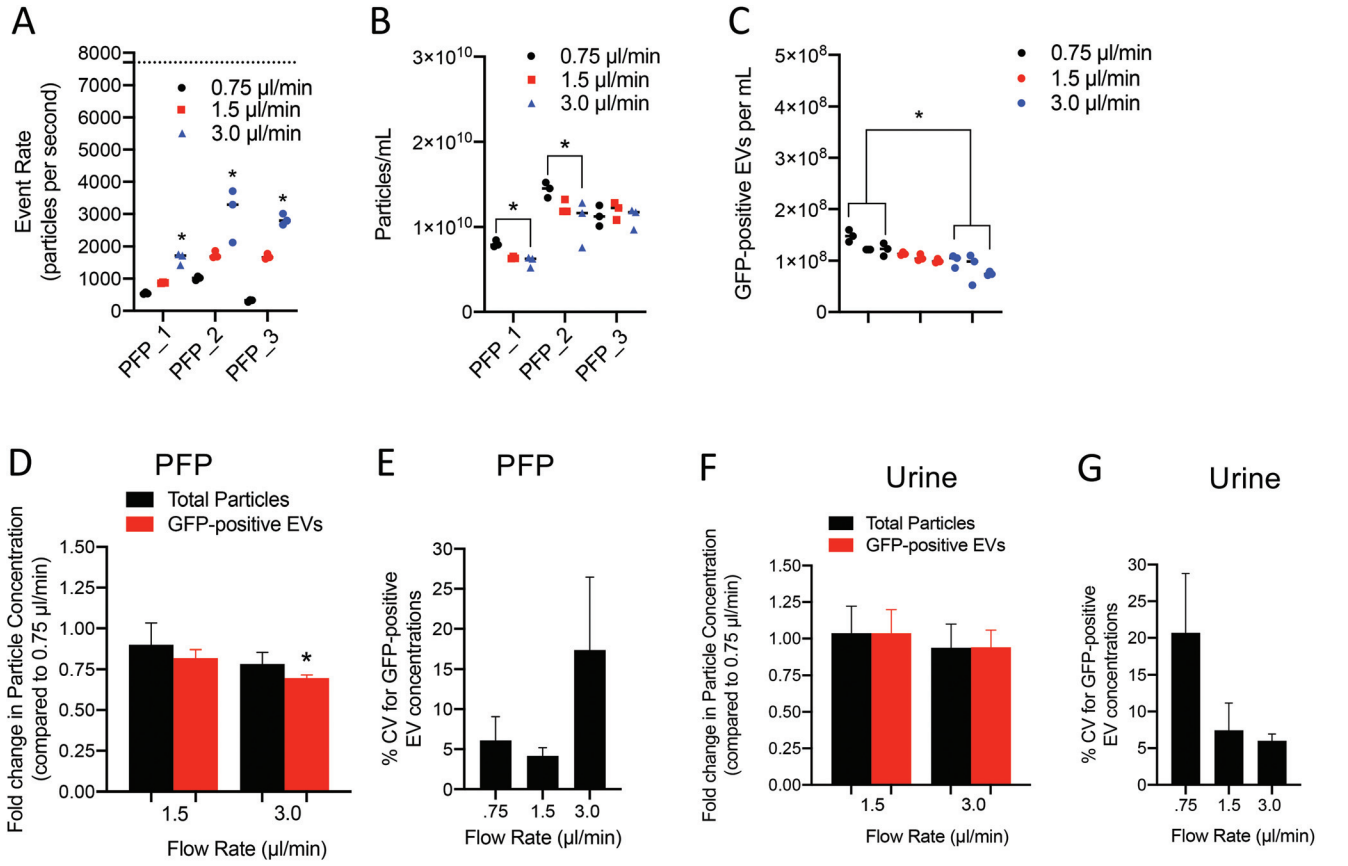

Fig. 4 Impact of flow rate on side scatter detection of particles and EVs from platelet-free plasma and cell-free urine. (A) Event rates of total particle detection per second from PFP (N = 3) measured in different sample flow rates. Flow rates are presented in µl min^{-1}. (B and C) Concentrations of total particles and GFP-positive rEVs detected from PFP with rEV spike-in (N = 3) measured in different sample flow rates. (D) Fold changes in detection levels of total particles and rEVs from rEV spiked-in PFP samples (N = 3) measured in different flow rates. Particle concentrations measured in flow rates 1.5 and 3.0 µl min^{-1} were normalized to the one measured in flow rates 0.75 µl min^{-1}. (E) The coefficient of variation of plasma GFP-positive rEV concentrations and total particle concentrations measured in different flow rates between each replicate. (F) Fold changes in detection levels of total particles and rEVs from rEV spiked-in urine samples (N = 3) measured in different flow rates. Particle concentrations measured in flow rates 1.5 and 3.0 µl min^{-1} were normalized to the one measured in flow rates 0.75 µl min^{-1}. (G) The coefficient of variation of urinary GFP-positive rEV concentrations measured in different flow rates between each replicate.

trary units corresponds to a scattering cross section of 9 nm^2 and an EV diameter of 158 nm.

Label-free detection and characterization of particles and EVs from blood and urine of prostate cancer patients and age-matched men with benign prostate hyperplasia

Using our standardized protocol and calibrated flow cytometer, we sought to determine concentration of particles in blood and urine of 85 prostate cancer patients and 35 men with benign prostate hyperplasia (BPH). We also employed refractive index-based discrimination (Flow-Scatter Ratio or Flow-SR) to distinguish EVs (RI < 1.45) from non-EV particles such as lipoproteins (RI > 1.45) in a label-free manner (Fig. 5A and B).[25,26]

Median particle concentration in plasma was similar in BPH patients and prostate cancer patients with 2.5 × 10^{10} and 3.0 × 10^{10} particles per ml respectively (Fig. S7C†). Using Flow-SR, we did not find any significant difference in concentrations of EVs and lipoproteins (LPs) between BPH and prostate cancer patients (Fig. 5C and D). In addition, the percentages of EVs were similar in prostate cancer patients compared to BPH patients (Fig. 5E).

In urine, no difference was observed in total particle concentration between BPH patients and prostate cancer patients with 1.1 × 10^9 particles per ml (Fig. S7D†). Most particles detected in urine (>89%) fell under a RI of 1.45 (Fig. 5F–H). When LPs were excluded from the analysis, median urine concentration of EVs was slightly higher in prostate cancer patients compared to BPH patients (1.3 × 10^8 *vs.* 9.1 × 10^7 particles per ml, p = 0.1702) (Fig. 5F). Percentages of EVs were similar in prostate cancer patients compared to BPH patients (Fig. 5H).

Antibody-based fluorescence detection of EVs in detection of prostate-derived EVs biofluids from BPH and prostate cancer patients

Our previous data show that label-free quantification of particles and EVs by flow cytometry is not sufficient to discrimi-

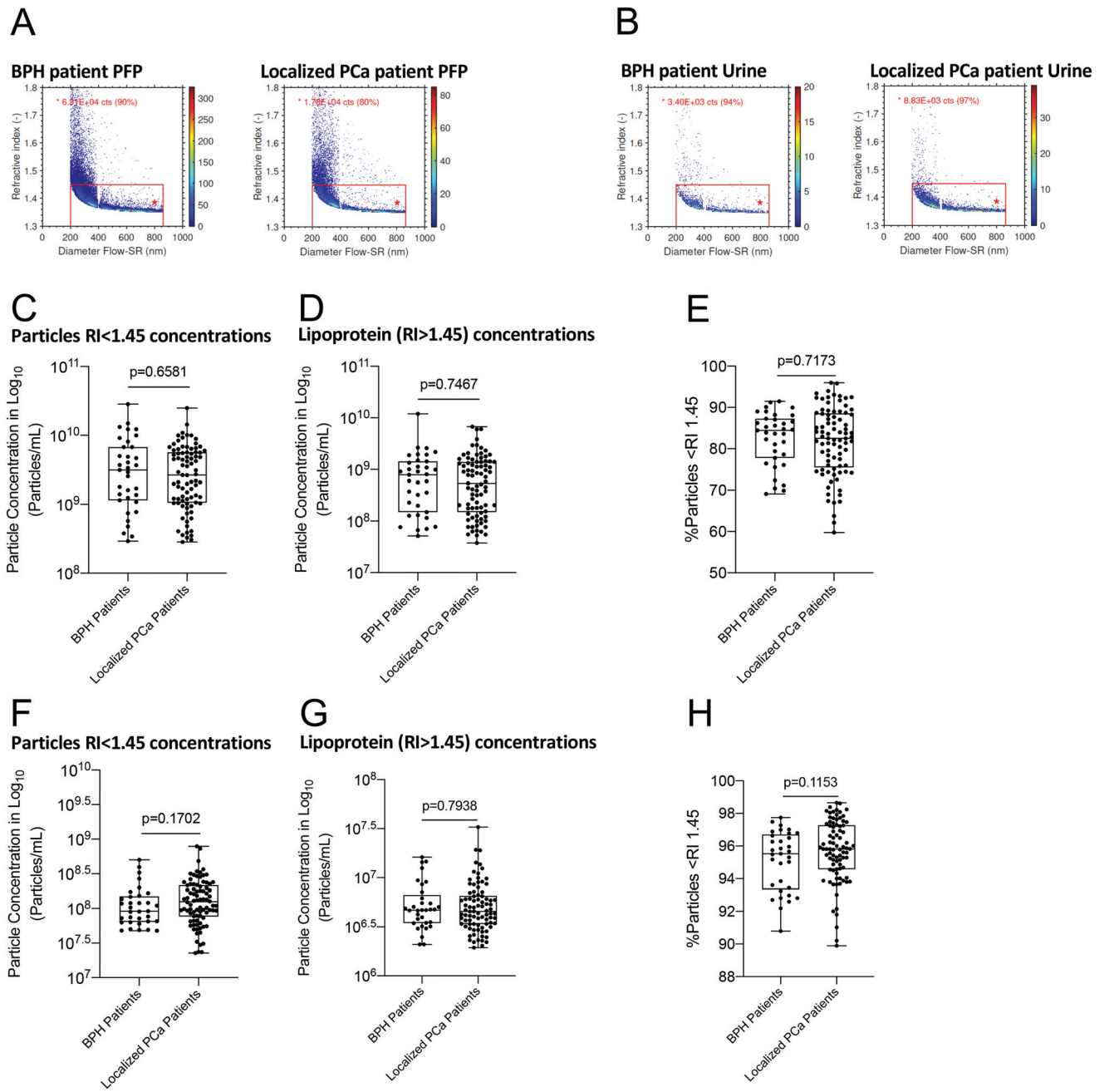

Fig. 5 Standardized label-free detection and characterization of EVs by refractive index from biofluids of localized prostate cancer patients and age-matched benign prostate hyperplasia (BPH) patients. (A and B) Representative cytograms showing EV (<RI 1.45) detection in plasma and urine samples of BPH (*N* = 35) and localized prostate cancer (*N* = 85) patients. (C and D) Comparison of particle and lipoprotein concentrations in plasma samples of BPH and localized prostate cancer patients. (E) Comparison of the percentages of particles in BPH and localized prostate cancer patient plasma samples. (F and G) Comparison of particle and lipoproteins in urine samples of BPH (*N* = 35) and localized prostate cancer (*N* = 85) patients. (H) Comparison of the percentages of particles with refractive index greater and less than 1.45 in urine samples of BPH and localized prostate cancer patients.

nate prostate cancer patients from men with BPH. Therefore, immunophenotyping using antibodies against tissue- or cancer-specific surface antigens is critical to further characterize the cellular source of EVs and identify potential diagnostic biomarkers. Accordingly, we measured the blood and urine levels of prostate-specific EVs using antibodies against two prostate markers, namely PSMA and STEAP1. To demonstrate the specificity of fluorescent antibodies in detecting EVs and not generating false-positive aggregates, we measured particle and EV concentrations in EV-depleted plasma (Fig. S8 and S9†). We used ultracentrifugation- and detergent-based methods to deplete EVs from human plasma. Using both

approaches, we observed a depletion of more than 90% of antibody-bound EVs which confirmed the specificity of PSMA and STEAP1 antibodies in binding EVs.

We compared the blood concentrations of $PSMA^+$-EVs and $STEAP1^+$-EVs between men with BPH, localized prostate cancer and metastatic castration-refractory prostate cancer (Fig. 6A and B). In addition, urine concentrations of both EV subsets were measured in men with BPH and localized prostate cancer (Fig. 6F and G). Similar levels of $PSMA^+$ and $STEAP1^+$ EVs were observed in both PFP and urine of prostate cancer patients and BPH men. However, blood concentrations of $PSMA^+$ EVs (8.4×10^6 *vs.* 3.8×10^6 and 2.9×10^6 Events per mL, $p < 0.01$) and $STEAP1^+$ EVs (9.6×10^7 *vs.* 2.0×10^7 and 1.6×10^7 Events per mL, $p < 0.0001$) were significantly higher in metastatic castration-refractory prostate cancer patients compared to both BPH and localized prostate cancer patients (Fig. 6B). In addition, there were significantly positive correlations between blood $PSMA^+$ EV levels and $STEAP1^+$ EV levels in both BPH ($r = 0.55$ and $p < 0.001$) and localized prostate cancer patients ($r = 0.45$ and $p < 0.0001$). A loss of positive correlation in blood $PSMA^+$ EV levels and $STEAP1^+$ EV levels was observed for metastatic prostate cancer patients ($r = -0.41$ and $p = 0.08$) (Fig. 6C–E). No difference was observed between BPH and localized prostate cancer for concentrations of urine-derived $PSMA^+$ EVs and $STEAP1^+$ EVs (Fig. 6F and G). Similar to blood, a strong and significantly positive correlation was observed between $PSMA^+$ EVs and $STEAP1^+$ EVs in urine of both BPH ($r = 0.80$ and $p < 0.0001$) and localized prostate cancer patients ($r = 0.69$ and $p < 0.0001$). (Fig. 6H and I). Antibody-based flow cytometric quantification of prostate-derived EVs using PSMA and STEAP1 markers do not distinguish men with localized prostate cancers from men with BPH. However, the significant increase in concentrations of both $PSMA^+$ EVs and $STEAP1^+$ EVs in metastatic prostate cancer patients suggest that prostate-derived EVs can serve as a surrogate marker of disease burden and identify patients with metastatic disease.

Discussion

In this study, we reported a systematic approach to identify the best acquisition parameters for quantification of biological particles and EVs in clinical platelet-free plasma and cell-free urine samples from healthy donors and prostate cancer patients using an A60-MicroPlus flow cytometer. To determine the optimal acquisition settings (illumination wavelength power, side scatter triggering threshold, flow rate) for sensitive detection of EVs without the need for fluorescent antibodies, we used recombinant fluorescent EVs (Gag-GFP) released by cultured cells and spiked-in biofluids. Recombinant EVs share similar biophysical properties as EVs released from wild-type cells and can serve as reliable test samples for EV-flow cytometry (Fig. S2D†).[28] Using rEV spiked-in biofluids, we observed that fine-tuning acquisition settings could substantially improve sensitivity for light scatter detection of small particles and technical replicability. Therefore, acquisition settings must be carefully selected based on the sample source and instrument capabilities while maintaining linear particle quantification.

Flow cytometry is the only method capable of quantifying, sizing, and characterizing millions of submicron particles in nanoscale sample volume and within minutes.[17] Besides being a valuable research tool to study EV biology and function in pathological conditions, flow cytometry is poised to play a pivotal role in the development of EV-based liquid biopsies for the management of human diseases.[29–31] However, single particle analysis remains challenging because EVs are a heterogeneous population of particles ranging from ~30 nanometers up to 5 micrometers with the majority of EVs falling under 300 nanometers. Each instrument also provides different sensitivity to detect submicron particles with extremely heterogenous sizes, which can result in significant discrepancy for the measured EV concentration.[16] Therefore, it is critical to standardize data acquisition by defining optimal instrumental settings for sensitive EV detection and quantification. In addition, instrument calibration with reference materials is also crucial for reporting data in standardized units so data can be compared with other platforms.[15] Finally, such rigorous and reproducible methodology will serve as framework for the development of new analytical tools and more sensitive flow cytometers.[22]

Once we identified optimal settings for plasma and urine analysis, we used the scatter-to-diameter relationship obtained by Mie theory to calibrate our flow cytometer and estimate absolute diameters and concentrations of particles and EVs in plasma and urine of prostate cancer patients.[12] Conversion of side scatter intensities from arbitrary units to nanometers is critical to assess the sensitivity of flow cytometers and allows inter-lab comparisons with similar or different instruments.[24] In this study, we employed Rosetta Calibration beads manufactured by Exometry Inc., which includes a software to transform side scatter intensities into diameter directly from raw flow cytometry files. Other manufactured NIST certified and traceable polystyrene and silica beads with known diameter and refractive index can be also used for similar purpose.[12] For example, FCM_{pass} software is another tool to convert side scatter intensities in diameter and includes fluorescence calibration as well.[32] Based on our instrument configuration and acquisition parameters, side scatter intensities recorded from a population of NIST polystyrene 80 nm beads corresponded to an EV with a mean diameter of 158 nm. Our A60MP flow cytometer was also capable of detecting recombinant Gag-GFP-positive EVs with a median diameter of 199 nm. Previous studies have reported a diameter for Gag-GFP-positive EVs of ~115 nm as measured by NTA and electron microscopy.[28,33] Discrepancy in size measurement can be explained by variability in instrument sensitivity but also in EV isolation methodology used. In our study, only dual centrifugation at 2500*g* was used to remove platelets, cellular debris, and aggregates. In both previous reports, density gradient and ultracentrifugation have been employed prior to size measurement which can result in enrichment of smaller particles.[28,33]

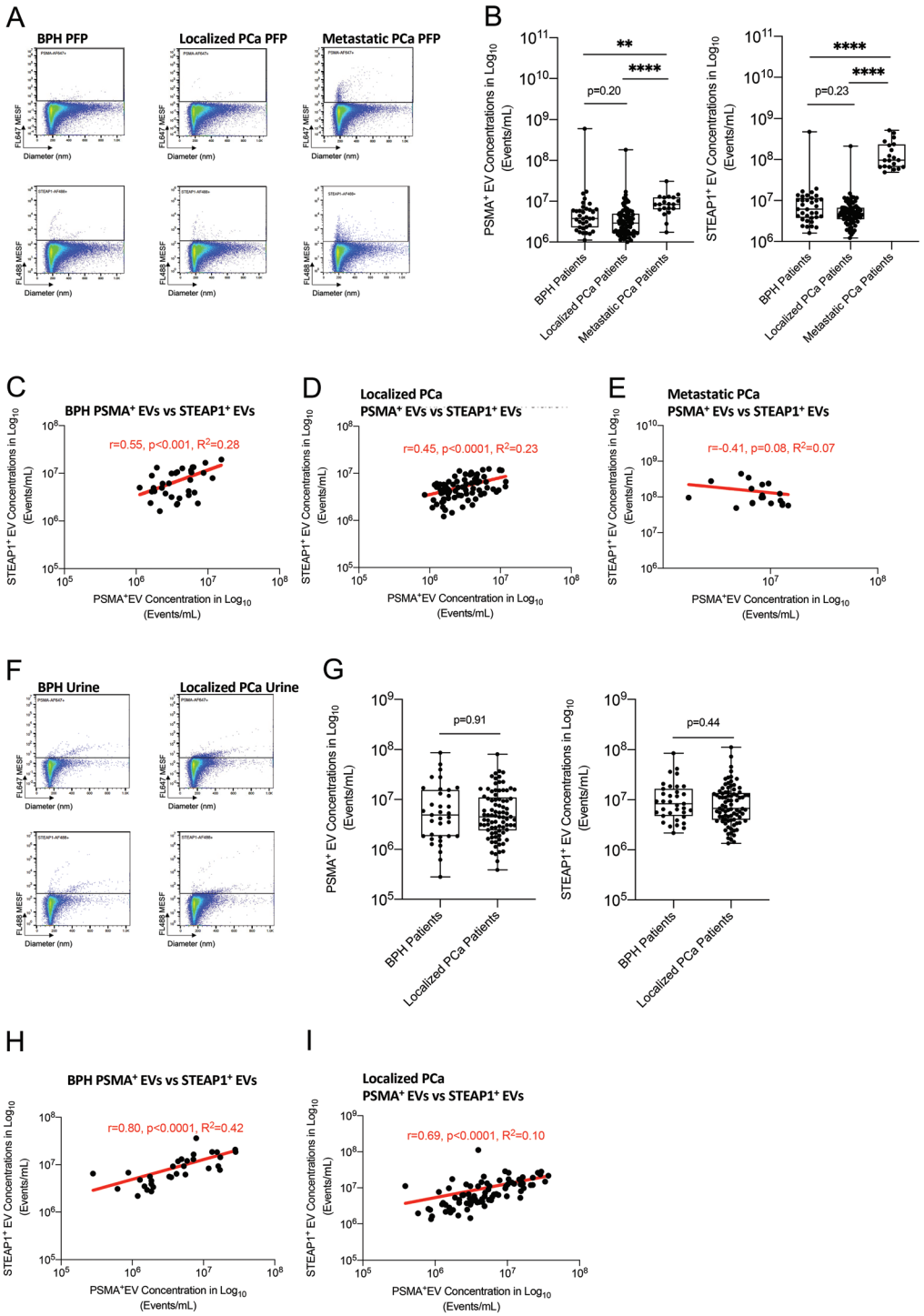

Fig. 6 Enumeration and characterization of fluorescent prostate cancer EVs in biofluids of localized prostate cancer patients and age-matched BPH patients. (A) Representative cytograms of $PSMA^+$ and $STEAP1^+$ EVs in plasma samples of BPH (N = 35), localized (N = 85) and metastatic (N = 20) prostate cancer patients. (B) The comparisons of $PSMA^+$ and $STEAP1^+$ EV levels in BPH (N = 35), localized (N = 85) and metastatic (N = 20) prostate cancer patient plasma samples. Kruskal–Wallis test, $^{**}p < 0.01$, $^{****}p < 0.0001$. (C–E) Correlations between $PSMA^+$ and $STEAP1^+$ EV levels from BPH, localized and metastatic prostate cancer patient plasma samples. (F) Representative cytograms of $PSMA^+$ and $STEAP1^+$ urinary EVs from BPH patients (N = 35) and localized prostate cancer patients (N = 85). (G) The comparisons of $PSMA^+$ and $STEAP1^+$ EV concentrations in urine samples of BPH patients (N = 35) and localized prostate cancer patients (N = 85). (H and I) Correlations between $PSMA^+$ and $STEAP1^+$ EV levels from BPH and localized prostate cancer patient urine samples.

To our knowledge, our study is the first to analyze concentration and size of particles and EVs from human plasma and matched urine using a standardized and calibrated flow cytometer and without the need for pre-enrichment/isolation. In a large cohort of specimens (N = 140), we reported a particle concentration in PFP ranging from 3.1×10^9 to 1.7×10^{11} particles per mL with a median particle concentration of 3.3×10^{10} particles per mL. In contrast, we found that circulating particles in urine are in lower concentration with a range from 1.1×10^8 to 2.0×10^9 particles per mL with a median particle concentration of 6.4×10^8 particles per mL (using similar acquisition settings for PFP and urine). Several reasons can explain the ~50-fold difference in particle concentration between both biofluid types. Blood contains concentrations of lipoproteins that exceed EV concentrations.[34] Among lipoproteins, chylomicrons share a similar light scatter property (*e.g.* diameter) to EVs and their abundance in blood is an important barrier for EV-FCM studies.[25,35,36] To avoid swarm detection, most PFP samples have been diluted at 200-fold in 200 microliters of PBS and run at a flow rate of 0.75 μl for 1 minute. This means that 0.0037 μl (3.7 nanoliters) of plasma are analyzed, which can result in limited sensitivity for low abundant EV populations such as organ- and cancer-specific EVs. Several methodologies have been developed to separate EVs from lipoproteins including size-exclusion chromatography and density-gradient centrifugation, but they are time-consuming, labor-intensive and require specific instrumentation.[37,38] Alternative pre-analytical strategies that can deplete lipoproteins from platelet-free plasma in a high-throughput manner are needed in order to improve flow cytometry sensitivity and its utility for EV research. As chylomicrons differ from EVs in terms of density and refractive index, both particle populations can be discriminated on flow cytometry by using side scatter intensity-refractive index relationship.[25,39] Herein, we provide the first external application of flow cytometry scatter ratio method (Flow-SR) in clinical cell-free plasma and urine samples. As expected, we observed a higher concentration of lipoproteins (particles with RI > 1.45) in plasma compared to urine. Besides the abundance of lipoproteins, other factors contribute to the differences in particle concentration between blood and urine. Urine-derived particles mostly originate from the urinary organs including bladder, kidney and prostate while hematopoietic and lymphatic systems and various epithelial tissues can contribute to the EV landscape in blood.[40,41] Additionally, urine is made from excess fluid and waste products eliminated from blood during glomerular filtration and the glomerular basement membrane is impermeant to particles larger than immunoglobulins in physiological conditions supporting the lower diversity in urine-derived EVs compared to blood.[42] EV-FCM combined with antibodies specific to tissue markers can be a method of choice to uncover the EV landscape in blood and urine and identify what organs release the most EVs in normal and pathological conditions.

Finally, we applied standardized and calibrated EV-FCM to compare particle concentration in biofluids from prostate cancer patients and men with benign prostatic hyperplasia. In the context of prostate cancer diagnosis, avoiding tissue biopsy to men with no prostate cancer is one of the biggest challenges in the management of prostate cancer.[43] Elevation of serum prostate specific antigen (PSA) remains the main clinical sign of prostate cancer. However, abnormal PSA levels can also be observed in men with benign prostatic hyperplasia or prostatitis, hence, poor specificity of PSA results in high false-positive rate (>50%) and unnecessary invasive biopsies. An EV-based blood or urine test using FCM is an attractive tool to improve prostate cancer diagnosis because it requires minimal instrumentation, minimal sample volume and results can be obtained within few hours. Few groups have used FCM to evaluate the potential role of EVs as diagnostic biomarker in prostate cancer.[11,44–47] To our knowledge, our study is the first to employ standardized and calibrated FCM for the quantification of particles and prostate-derived EVs from blood and urine. Furthermore, we compared side-by-side two prostate markers, namely PSMA and STEAP1.[48] For both blood and urine, we did not find significant difference in total particle number as well as in concentrations of $PSMA^+$-EVs between BPH and localized prostate cancer which corroborates with two previous studies.[45,47] We obtained similar findings with STEAP1 marker which suggest that tissue-specific EV markers are not sufficient to discriminate localized cancer patients from men with BPH. Interestingly, we found a significant elevation of $PSMA^+$-EVs and $STEAP1^+$-EVs in metastatic castration-refractory prostate cancer (mCRPC) compared to localized prostate cancer and BPH. This cohort consists of patients who are refractory to prior systemic therapies and present with high metastatic burden on CT/bone scan imaging. Our data suggest that blood levels of $PSMA^+$-EVs and $STEAP1^+$-EVs may serve as prognostic biomarkers in prostate cancer. Although significant differences were observed in levels of $PSMA^+$-EVs and $STEAP1^+$-EVs between mCRPC and localized prostate cancer, we simultaneously observed that the correlation between $PSMA^+$-EVs and $STEAP1^+$-EVs was lost and $STEAP1^+$-EVs outnumbered $PSMA^+$-EVs in mCRPC patient samples. Lower PSMA expression has been previously reported in treatment-refractory prostate cancer patients.[49–54] In response to androgen-deprivation therapy, CRPC tumors can progress towards a neuroendocrine phenotype and lose PSMA expression. Herein, we provide blood-based evidence that both $PSMA^+$ and $STEAP1^+$-EVs can be promising for identification of aggressive prostate cancer including those characterized by neuroendocrine features and low serum PSA levels.

Conclusion

This study underlines the feasibility and relevance to standardize and calibrate EV-FCM using the most recent guidelines from the EV-FCM Working Group and the ISEV community. By reporting detailed methodologies, instrument characteristics and acquisition settings, our work can serve as a framework for inter-lab comparison studies and further investigate the

clinical utility of prostate-derived EVs as liquid biomarkers for the management of prostate cancer.

Data availability

The datasets and patient-level data supporting this article have been uploaded as part of the ESI.† Raw flow cytometry data files are available via Figshare **https://figshare.com/projects/Kim_Y_et_al_2022_Calibration_and_Standardization_of_Extracellular_Vesicle_Measurements_by_Flow_Cytometry_for_Translational_Prostate_Cancer_Research/138135**

Author contributions

F. L. conceptualized the study. Y. K., E. P., A. A., S. S., I. T., F. L. performed and analyzed experiments. C. B. collected demographics and clinical characteristics. R. E. and V. B. J. oversee the clinical study protocol and consented patients for the study. Y. K. and F. L. wrote the first draft of the manuscript. All the authors reviewed and approved the manuscript.

Conflicts of interest

E. van der Pol is co-founder and shareholder of Exometry BV.

Acknowledgements

This work was supported by departmental start-up grant (F. L.) and generous benefactors (F. L.). We also thank generous patients who have participated to the study by providing biospecimens.

References

1 R. Shah, T. Patel and J. E. Freedman, Circulating Extracellular Vesicles in Human Disease, *N. Engl. J. Med.*, 2018, **379**(10), 958–966.
2 C. Thery, K. W. Witwer, E. Aikawa, M. J. Alcaraz, J. D. Anderson, R. Andriantsitohaina, *et al.*, Minimal information for studies of extracellular vesicles 2018 (MISEV2018): a position statement of the International Society for Extracellular Vesicles and update of the MISEV2014 guidelines, *J. Extracell. Vesicles*, 2018, **7**(1), 1535750.
3 S. L. N. Maas, X. O. Breakefield and A. M. Weaver, Extracellular Vesicles: Unique Intercellular Delivery Vehicles, *Trends Cell Biol.*, 2017, **27**(3), 172–188.
4 A. J. Vickers, D. D. Sjoberg, D. Ulmert, E. Vertosick, M. J. Roobol, I. Thompson, *et al.*, Empirical estimates of prostate cancer overdiagnosis by age and prostate-specific antigen, *BMC Med.*, 2014, **12**, 26.
5 T. Nordstrom, A. Discacciati, M. Bergman, M. Clements, M. Aly, M. Annerstedt, *et al.*, Prostate cancer screening using a combination of risk-prediction, MRI, and targeted prostate biopsies (STHLM3-MRI): a prospective, population-based, randomised, open-label, non-inferiority trial, *Lancet Oncol.*, 2021, **22**(9), 1240–1249.
6 R. J. Rebello, C. Oing, K. E. Knudsen, S. Loeb, D. C. Johnson, R. E. Reiter, *et al.*, Prostate cancer, *Nat. Rev. Dis. Primers*, 2021, **7**(1), 9.
7 F. A. W. Coumans, A. R. Brisson, E. I. Buzas, F. Dignat-George, E. E. E. Drees, S. El-Andaloussi, *et al.*, Methodological Guidelines to Study Extracellular Vesicles, *Circ. Res.*, 2017, **120**(10), 1632–1648.
8 J. Li, H. Liu, A. S. Mauer, F. Lucien, A. Raiter, H. Bandla, *et al.*, Characterization of Cellular Sources and Circulating Levels of Extracellular Vesicles in a Dietary Murine Model of Nonalcoholic Steatohepatitis, *Hepatol. Commun.*, 2019, **3**(9), 1235–1249.
9 F. Lucien, V. Lac, D. D. Billadeau, A. Borgida, S. Gallinger and H. S. Leong, Glypican-1 and glycoprotein 2 bearing extracellular vesicles do not discern pancreatic cancer from benign pancreatic diseases, *Oncotarget*, 2019, **10**(10), 1045–1055.
10 D. Choi, L. Montermini, H. Jeong, S. Sharma, B. Meehan and J. Rak, Mapping Subpopulations of Cancer Cell-Derived Extracellular Vesicles and Particles by Nano-Flow Cytometry, *ACS Nano*, 2019, **13**(9), 10499–10511.
11 K. Khanna, N. Salmond, K. S. Lynn, H. S. Leong and K. C. Williams, Clinical significance of STEAP1 extracellular vesicles in prostate cancer, *Prostate Cancer Prostatic Dis.*, 2021, **24**(3), 802–811.
12 L. de Rond, F. A. W. Coumans, R. Nieuwland, T. G. van Leeuwen and E. van der Pol, Deriving Extracellular Vesicle Size From Scatter Intensities Measured by Flow Cytometry, *Curr. Protoc. Cytom.*, 2018, **86**(1), e43.
13 G. J. A. Arkesteijn, E. Lozano-Andres, S. Libregts and M. H. M. Wauben, Improved Flow Cytometric Light Scatter Detection of Submicron-Sized Particles by Reduction of Optical Background Signals, *Cytometry, Part A*, 2020, **97**(6), 610–619.
14 A. Gorgens, M. Bremer, R. Ferrer-Tur, F. Murke, T. Tertel, P. A. Horn, *et al.*, Optimisation of imaging flow cytometry for the analysis of single extracellular vesicles by using fluorescence-tagged vesicles as biological reference material, *J. Extracell. Vesicles*, 2019, **8**(1), 1587567.
15 J. A. Welsh, E. van der Pol, B. A. Bettin, D. R. F. Carter, A. Hendrix, M. Lenassi, *et al.*, Towards defining reference materials for measuring extracellular vesicle refractive index, epitope abundance, size and concentration, *J. Extracell. Vesicles*, 2020, **9**(1), 1816641.
16 E. van der Pol, A. Sturk, T. van Leeuwen, R. Nieuwland, F. Coumans and I.-S.-V. W. Group, Standardization of extracellular vesicle measurements by flow cytometry through vesicle diameter approximation, *J. Thromb. Haemostasis*, 2018, **16**(6), 1236–1245.

17 J. Gomes, F. Lucien, T. T. Cooper, Y. Kim, K. C. Williams, X. Liao, *et al.*, Analytical Considerations in Nanoscale Flow Cytometry of Extracellular Vesicles to Achieve Data Linearity, *Thromb. Haemostasis*, 2018, **118**(9), 1612–1624.

18 S. Deville, P. Berckmans, R. Van Hoof, I. Lambrichts, A. Salvati and I. Nelissen, Comparison of extracellular vesicle isolation and storage methods using high-sensitivity flow cytometry, *PLoS One*, 2021, **16**(2), e0245835.

19 T. Tertel, M. Bremer, C. Maire, K. Lamszus, S. Peine, R. Jawad, *et al.*, High-Resolution Imaging Flow Cytometry Reveals Impact of Incubation Temperature on Labeling of Extracellular Vesicles with Antibodies, *Cytometry, Part A*, 2020, **97**(6), 602–609.

20 L. de Rond, E. van der Pol, P. R. Bloemen, T. Van Den Broeck, L. Monheim, R. Nieuwland, *et al.*, A Systematic Approach to Improve Scatter Sensitivity of a Flow Cytometer for Detection of Extracellular Vesicles, *Cytometry, Part A*, 2020, **97**(6), 582–591.

21 L. de Rond, F. A. W. Coumans, J. A. Welsh, R. Nieuwland, T. G. van Leeuwen and E. van der Pol, Quantification of Light Scattering Detection Efficiency and Background in Flow Cytometry, *Cytometry, Part A*, 2021, **99**(7), 671–679.

22 J. A. Welsh, E. Van Der Pol, G. J. A. Arkesteijn, M. Bremer, A. Brisson, F. Coumans, *et al.*, MIFlowCyt-EV: a framework for standardized reporting of extracellular vesicle flow cytometry experiments, *J. Extracell. Vesicles*, 2020, **9**(1), 1713526.

23 J. A. Welsh, V. A. Tang, E. van der Pol and A. Gorgens, MIFlowCyt-EV: The Next Chapter in the Reporting and Reliability of Single Extracellular Vesicle Flow Cytometry Experiments, *Cytometry, Part A*, 2021, **99**(4), 365–368.

24 J. A. Welsh, J. C. Jones and V. A. Tang, Fluorescence and Light Scatter Calibration Allow Comparisons of Small Particle Data in Standard Units across Different Flow Cytometry Platforms and Detector Settings, *Cytometry, Part A*, 2020, **97**(6), 592–601.

25 E. van der Pol, L. de Rond, F. A. W. Coumans, E. L. Gool, A. N. Boing, A. Sturk, *et al.*, Absolute sizing and label-free identification of extracellular vesicles by flow cytometry, *Nanomedicine*, 2018, **14**(3), 801–810.

26 D. Ducharme, J. J. Max, C. Salesse and R. M. Leblanc, Ellipsometric study of the physical states of phosphatidylcholines at the air-water interface, *J. Phys. Chem.*, 1990, **94**(5), 1925–1932.

27 E. van der Pol, M. J. van Gemert, A. Sturk, R. Nieuwland and T. G. van Leeuwen, Single vs, swarm detection of microparticles and exosomes by flow cytometry, *J. Thromb. Haemostasis*, 2012, **10**(5), 919–930.

28 E. Geeurickx, J. Tulkens, B. Dhondt, J. Van Deun, L. Lippens, G. Vergauwen, *et al.*, The generation and use of recombinant extracellular vesicles as biological reference material, *Nat. Commun.*, 2019, **10**(1), 3288.

29 M. Kuiper, A. van de Nes, R. Nieuwland, Z. Varga and E. van der Pol, Reliable measurements of extracellular vesicles by clinical flow cytometry, *Am. J. Reprod. Immunol.*, 2021, **85**(2), e13350.

30 A. Gasecka, M. Banaszkiewicz, R. Nieuwland, E. van der Pol, N. Hajji, H. Mutwil, *et al.*, Prostacyclin Analogues Inhibit Platelet Reactivity, Extracellular Vesicle Release and Thrombus Formation in Patients with Pulmonary Arterial Hypertension, *J. Clin. Med.*, 2021, **10**(5), 1024.

31 N. Salmond, K. Khanna, G. R. Owen and K. C. Williams, Nanoscale flow cytometry for immunophenotyping and quantitating extracellular vesicles in blood plasma, *Nanoscale*, 2021, **13**(3), 2012–2025.

32 J. A. Welsh, P. Horak, J. S. Wilkinson, V. J. Ford, J. C. Jones, D. Smith, *et al.*, FCMPASS Software Aids Extracellular Vesicle Light Scatter Standardization, *Cytometry, Part A*, 2020, **97**(6), 569–581.

33 D. Fontana, E. Garay, L. Cervera, R. Kratje, C. Prieto and F. Godia, Chimeric VLPs Based on HIV-1 Gag and a Fusion Rabies Glycoprotein Induce Specific Antibodies against Rabies and Foot-and-Mouth Disease Virus, *Vaccines*, 2021, **9**(3), 251.

34 K. B. Johnsen, J. M. Gudbergsson, T. L. Andresen and J. B. Simonsen, What is the blood concentration of extracellular vesicles? Implications for the use of extracellular vesicles as blood-borne biomarkers of cancer, *Biochim. Biophys. Acta, Rev. Cancer*, 2019, **1871**(1), 109–116.

35 B. W. Sodar, A. Kittel, K. Paloczi, K. V. Vukman, X. Osteikoetxea, K. Szabo-Taylor, *et al.*, Low-density lipoprotein mimics blood plasma-derived exosomes and microvesicles during isolation and detection, *Sci. Rep.*, 2016, **6**, 24316.

36 L. de Rond, S. Libregts, L. G. Rikkert, C. M. Hau, E. van der Pol, R. Nieuwland, *et al.*, Refractive index to evaluate staining specificity of extracellular vesicles by flow cytometry, *J. Extracell. Vesicles*, 2019, **8**(1), 1643671.

37 K. Brennan, K. Martin, S. P. FitzGerald, J. O'Sullivan, Y. Wu, A. Blanco, *et al.*, A comparison of methods for the isolation and separation of extracellular vesicles from protein and lipid particles in human serum, *Sci. Rep.*, 2020, **10**(1), 1039.

38 X. Zhang, E. G. F. Borg, A. M. Liaci, H. R. Vos and W. Stoorvogel, A novel three step protocol to isolate extracellular vesicles from plasma or cell culture medium with both high yield and purity, *J. Extracell. Vesicles*, 2020, **9**(1), 1791450.

39 E. van der Pol, F. A. Coumans, A. Sturk, R. Nieuwland and T. G. van Leeuwen, Refractive index determination of nanoparticles in suspension using nanoparticle tracking analysis, *Nano Lett.*, 2014, **14**(11), 6195–6201.

40 B. Dhondt, E. Geeurickx, J. Tulkens, J. Van Deun, G. Vergauwen, L. Lippens, *et al.*, Unravelling the proteomic landscape of extracellular vesicles in prostate cancer by density-based fractionation of urine, *J. Extracell. Vesicles*, 2020, **9**(1), 1736935.

41 A. Hoshino, H. S. Kim, L. Bojmar, K. E. Gyan, M. Cioffi, J. Hernandez, *et al.*, Extracellular Vesicle and Particle Biomarkers Define Multiple Human Cancers, *Cell*, 2020, **182**(4), 1044–1061.e18.

42 M. G. Lawrence, M. K. Altenburg, R. Sanford, J. D. Willett, B. Bleasdale, B. Ballou, *et al.*, Permeation of macromolecules into the renal glomerular basement membrane and capture by the tubules, *Proc. Natl. Acad. Sci. U. S. A.*, 2017, **114**(11), 2958–2963.

43 N. J. Sathianathen, K. M. Kuntz, F. Alarid-Escudero, N. L. Lawrentschuk, D. M. Bolton, D. G. Murphy, *et al.*, Incorporating Biomarkers into the Primary Prostate Biopsy Setting: A Cost-Effectiveness Analysis, *J. Urol.*, 2018, **200**(6), 1215–1220.

44 M. Logozzi, D. F. Angelini, E. Iessi, D. Mizzoni, R. Di Raimo, C. Federici, *et al.*, Increased PSA expression on prostate cancer exosomes in in vitro condition and in cancer patients, *Cancer Lett.*, 2017, **403**, 318–329.

45 C. N. Biggs, K. M. Siddiqui, A. A. Al-Zahrani, S. Pardhan, S. I. Brett, Q. Q. Guo, *et al.*, Prostate extracellular vesicles in patient plasma as a liquid biopsy platform for prostate cancer using nanoscale flow cytometry, *Oncotarget*, 2016, **7**(8), 8839–8849.

46 L. G. Rikkert, L. de Rond, A. van Dam, T. G. van Leeuwen, F. A. W. Coumans, T. M. de Reijke, *et al.*, Detection of extracellular vesicles in plasma and urine of prostate cancer patients by flow cytometry and surface plasmon resonance imaging, *PLoS One*, 2020, **15**(6), e0233443.

47 R. S. Padda, F. K. Deng, S. I. Brett, C. N. Biggs, P. N. Durfee, C. J. Brinker, *et al.*, Nanoscale flow cytometry to distinguish subpopulations of prostate extracellular vesicles in patient plasma, *Prostate*, 2019, **79**(6), 592–603.

48 J. K. Lee, N. J. Bangayan, T. Chai, B. A. Smith, T. E. Pariva, S. Yun, *et al.*, Systemic surfaceome profiling identifies target antigens for immune-based therapy in subtypes of advanced prostate cancer, *Proc. Natl. Acad. Sci. U. S. A.*, 2018, **115**(19), E4473–E4E82.

49 S. P. Thang, J. Violet, S. Sandhu, A. Iravani, T. Akhurst, G. Kong, *et al.*, Poor Outcomes for Patients with Metastatic Castration-resistant Prostate Cancer with Low Prostate-specific Membrane Antigen (PSMA) Expression Deemed Ineligible for (177)Lu-labelled PSMA Radioligand Therapy, *Eur. Urol. Oncol.*, 2019, **2**(6), 670–676.

50 L. Emmett, M. Crumbaker, B. Ho, K. Willowson, P. Eu, L. Ratnayake, *et al.*, Results of a Prospective Phase 2 Pilot Trial of (177)Lu-PSMA-617 Therapy for Metastatic Castration-Resistant Prostate Cancer Including Imaging Predictors of Treatment Response and Patterns of Progression, *Clin. Genitourin. Cancer*, 2019, **17**(1), 15–22.

51 J. Schwenck, H. Rempp, G. Reischl, S. Kruck, A. Stenzl, K. Nikolaou, *et al.*, Comparison of (68)Ga-labelled PSMA-11 and (11)C-choline in the detection of prostate cancer metastases by PET/CT, *Eur. J. Nucl. Med. Mol. Imaging*, 2017, **44**(1), 92–101.

52 M. K. Bakht, I. Derecichei, Y. Li, R. M. Ferraiuolo, M. Dunning, S. W. Oh, *et al.*, Neuroendocrine differentiation of prostate cancer leads to PSMA suppression, *Endocr.-Relat. Cancer*, 2018, **26**(2), 131–146.

53 H. Beltran, A. Hruszkewycz, H. I. Scher, J. Hildesheim, J. Isaacs, E. Y. Yu, *et al.*, The Role of Lineage Plasticity in Prostate Cancer Therapy Resistance, *Clin. Cancer Res.*, 2019, **25**(23), 6916–6924.

54 S. McGeorge, M. Kwok, A. Jiang, L. Emmett, D. A. Pattison, P. A. Thomas, *et al.*, Dual-Tracer Positron-Emission Tomography Using Prostate-Specific Membrane Antigen and Fluorodeoxyglucose for Staging of Prostate Cancer: A Systematic Review, *Adv. Urol.*, 2021, **2021**, 1544208.